MULTI-INSECT VISUAL TRACKING AND SYSTEM IDENTIFICATION TECHNIQUES FOR INFLIGHT FEEDBACK INTERACTION ANALYSIS

By

ISHRIAK AHMED

Bachelor of Science in Mechanical Engineering
Bangladesh University of Engineering and Technology
Dhaka, Bangladesh
2017

Submitted to the Faculty of the
Graduate College of the
Oklahoma State University
in partial fulfillment of
the requirements for
the Degree of
MASTER OF SCIENCE
July, 2021

MULTI-INSECT VISUAL TRACKING AND SYSTEM IDENTIFICATION TECHNIQUES FOR INFLIGHT FEEDBACK INTERACTION ANALYSIS

Thesis Approved:

Dr. Imraan Faruque

Thesis Adviser

Dr. He Bai

Dr. Guoliang Fan

ACKNOWLEDGMENTS

In the name of Allah the most merciful and most gracious...

I owe my gratitude to Allah for all the blessings he has bestowed upon me. I am lucky to be given a chance to study his marvellous creations.

I am grateful for my family, who made their sacrifices to make me what I am today. For my mother, who never stops thinking about what is the best for me. For my father, who always supported me in all my endeavours. For my brother, who was by their side when I could not. I am thankful to my wife, for worrying,preparing for my newborn baby when I was busy working in lab and for being an amazing supportive partner. I am thankful to my friends who were always there for me.

I am thankful to my advisor Dr. Faruque for guiding me when I was puzzled and all my colleagues in the lab who helped me with their brilliant ideas and friendship.

Acknowledgments reflect the views of the author and are not endorsed by committee members or Oklahoma State University.

Name: ISHRIAK AHMED

Date of Degree: JULY, 2021

Title of Study: MULTI-INSECT VISUAL TRACKING AND SYSTEM IDENTIFICATION TECHNIQUES FOR INFLIGHT FEEDBACK INTERACTION ANALYSIS

Major Field: MECHANICAL AND AEROSPACE ENGINEERING

Abstract: Individual insects flying in crowded assemblies perform complex aerial maneuvers by small changes in their wing motions. To understand the individual feedback rules that permit these fast, adaptive behaviors in group flight, a high-speed tracking system is needed that is capable of simultaneously tracking both body motions and these more subtle wing motion changes for multiple insects, extending tracking beyond the previous focus on individual insects to multiple insects. In this system, we have extended our capability to track multiple insects using high speed cameras (9000 fps). To improve the biological validity of laboratory experiments, we tested this measurement system with *Apis mellifera* foragers habituated to transit flights through a test chamber. Processing steps consist of data association, hull reconstruction, and segmentation. An analysis based on multiple flight trajectories is presented, including the differences in flight in open and confined areas containing multiple insects and the differences due to ethanol treatment. A system identification framework applicable to extracting the interaction rules in multi-agent insect trajectories is developed.

TABLE OF CONTENTS

Chapter Page

LIST OF TABLES

LIST OF FIGURES

Figure Page

CHAPTER I

INTRODUCTION

The growing application of small-scale unmanned aerial systems has created a need for sensing and feedback paths that provide computationally-efficient, robust autonomy. The need for computationally-constrained robust autonomy is especially demanding in the case of small aerial platforms appropriate for swarm use, where size, weight, and power constraints limit the sensor payloads, processing, and communication tools that can be carried.

Insects are model systems for this challenge as they achieve robust maneuvers in unpredictable dynamic environment despite relatively limited neural resources. This performance includes multi-agent behaviors such as cohesion, swarming, and other coordinated motions involving navigation relative to each other. They often achieve these relative navigation tasks by means of implicit visual communication, i.e., without explicit communication links.

Despite these advantages, many attempts to replicate insect swarm behaviors have suffered from a lack of precise measurements quantifying their relative motion behaviors, and these bio-inspired routines are then inspired at the outline level rather than experimentally consistent. The degree to which they are biological consistent limits the resolution of the approaches; consequently, they often have not yet achieved the robustness seen in biological implementations.

Early work quantified the positions of insects as point masses, tracking only their positions. Recent high speed recording and visual tracking tools have enabled solitary insect measurements that include wing motions, which includes rigid and flexible body

digitization of body and wing positions. Automated tracking has led to improvements in our understanding of the sensing and feedback paths used in individual flight control, including quantification of the flight stabilization reflex, and of the reward/penalty functions that insects feedback laws encode.

Detailed measurements of wing and body motion are needed in the multi-insect case to provide tools to extract the actual interaction rules implemented by swarming insects. These measurements need to precisely quantify the small perturbations in the moving motion, including increasing the tracked volume to allow for multiple interacting insects.

This paper introduces a multi-insect, high speed tracker that simultaneously digitizes the flight trajectories of a flexible number of insects, including position and orientation for body and wings. High speed Visual Insect Swarm Tracking (Hi-VISTA) is able to handle a flexible number and orientation of cameras and achieves improved throughput by parallel processing on several workstations. Hi-VISTA is tested on two candidate test studies.

The first study examines the effect of insect confinement. Although progress has been made in moving from tethered to free flight, the high lighting requirements and low depth of field of high speed cameras has typically limited measurement to small flight enclosures. The effect of these enclosures is not yet well quantified.

Because social interactions may be a strong component of the in-flight interaction rules in swarm and group behaviors, mechanisms that can manipulate these tools will improve the accuracy of system identification or "black box" tools to extract these rules. Ethanol has shown several effects on honeybees in terrestrial experiments, including changes in puzzle solving, aggressiveness, and the degree of social interaction. The second manipulation examines the kinematic effects of ethanol treatment in honeybees.

The study comprises 93 flight trials. 15 variables are tracked for each case, including

body states and gross wing motion parameters such as stroke amplitude. In both manipulations, the variables are analyzed by considering the trial wide mean and maximum values, and testing for statistical significance using ANOVA, Welch's t-test, and Cohen's d test. Then we present some system identification frameworks which may be used for analyse behaviour of insects in a group context.

CHAPTER II

PREVIOUS WORKS

2.1 High Speed Visual Insect trackers

Various approaches have been taken to study insect in flight kinematics by resolving their body and wing orientation in the past. To study non-tethered free flight typically a multi camera setup is necessary to gain depth information. (Fry et al., 2003) used manual methods where multiple landmarks on a fly are digitized by using orthogonal multiple camera views. (Hedrick, 2008) used direct linear coefficients camera calibration which can work with more flexible camera settings not requiring orthogonality. Usage of manual landmark based trackers are limited to insects big enough to use markers on without changing their flight dynamics. Among the automatic trackers (Ristroph et al., 2009) introduced Hull Reconstruction Motion Tracking which uses three orthogonal views extruded to produce maximally consistent 3D pixels (voxel). (Kostreski, 2012), used DLT coefficients with Hull reconstruction techniques removing the restriction of camera orthogonality. (Grover et al., 2008) made real-time tracker to track body states of multiple flies. (Fontaine et al., 2009) attempted model-based tracking in which tracking is initialized manually by superimposing a predefined insect model. Studies on multiple insect flights have been limited to position and orientation tracking with no information on wing motion. In continuity of previous works the main contribution in this paper is that we implemented a modified association routine based on (Straw et al., 2011) and extended the capabilities of a single insect tracker to a multi-insect one to track the wing states as well. We have built on works of (Kostreski, 2012) which does not need manual initialization or a fixed insect model because in the multi

insect environment the number of targets may change in different time frames, targets can get lost and and reappear, and they may have different body orientation resulting in repeated initialization process.

2.1.1 Wide area visual position tracking

(Straw et al., 2011) build Flydra to track fruit flies and hummingbirds that allows tracking in large areas of space in real-time. They used constructed the 3D position of the animal from multiple 2D views by finding the intersection of emerging lines and implementing nearest neighbor algorithm with an EKF. (Grover et al., 2008) uses multiple silhouettes to construct 3D visual hull of a fly, and tracks the multiple hulls in real-time with EKF implementation. (Ardekani et al., 2013) developed a program to keep track of multiple flies in a 3D arena for a long period of time (hours) enabling individual behavioral analysis.

To track individual insects, appearance features such as color and shapes have been used for identifying individuals in data-association(Kuo et al., 2010)(Zhou et al., 2004).

2.2 Studies on ethanol-exposed honey bees

Honey bees have much to recommend them for studies of ethanol induced behavior. Bees have low procurement and maintenance costs, a vast database for information on natural history, physiology, and genetics. Moreover, bees engage in a wide range of simple and complex behaviors including learning, communication, and the capacity to self-administer large quantity of ethanol (Bozic et al., 2007).

Much like humans, honey bees can have alcohol naturally in their diet as they forage on fermenting nectar and fruit, but unlike fruit flies humans and honey bees do not have a life stage dependent on alcohol (Gibson et al., 1981). Honey bees easily consume high quantities and concentrations of alcohol and, like humans, demonstrate

preferences for specific types of alcohol (Abramson et al., 2004b). Further, bees and humans exhibit similar aggression, locomotor, and learning changes following ethanol consumption (Abramson et al., 2004a)(Giannoni-Guzmán et al., 2014).

Honey bees become more aggressive under ethanol exposure (Abramson et al., 2004a)(Giannoni-Guzmán et al., 2014), showing a decreased threshold for the sting extension response after ethanol consumption (Giannoni-Guzmán et al., 2014). Following the consumption of an ethanol solution, honey bees would sting a leather patch en masse more often than bees that consumed a simple sucrose solution (Abramson et al., 2004a).

Bees like humans also show alcohol dose-dependent decreases in locomotor activity (Abramson et al., 2000). Consuming small quantities of ethanol causes bees to display erratic movements (Mixson et al., 2010). Additionally, high EtOH doses produces decreases in both bee flight and walking activity(Bozic et al., 2007)(Maze et al., 2006).

After consuming high quantities of ethanol humans often suffer from learning and memory impairments. Alcohol dose-dependent learning impairments are seen as well in honey bees (Abramson et al., 2000)(Abramson et al., 2005)(Abramson et al., 2015), even in learning tasks as simple as association between an odor (CS) and a sucrose reward (US) in proboscis extension response (PER) experiments e.g. (Abramson et al., 2000).

All these studies suggest that general honey bee behaviour is changed under ethanol influence, and their flight behaviour may potentially be impacted as well. In this work we conduct some simple analyses to guide us to reveal these effects.

CHAPTER III

MULTI-INSECT TRACKER

In this section the main construction of the Multi insect tracker is described. The tracking program requires the DLT camera calibration matrices (Abdel-Aziz et al., 2015) as an input in order to operate. The main program is built in four major sections described in 3.2 - 3.5. A flowchart of the main program is shown in Figure 3.1. Inspirations of the methods are taken from previous literature. However there are several implementation modifications to make it robust to the variety of data measured in multi agent flight.

3.1 Camera Calibration

Camera calibration allows us to mathematically relate a 3D point in world to the 2D point in an image formed by the camera. Pinhole camera model approximate imaging process by projecting objects through a point. 3D – 2D correspondence can be described using camera projection matrix L, which is dependent on camera properties and position of camera in the world coordinate system. The goal of multi-camera calibration program is to estimate the matrix L. As points in 3D world are quantized in pixels when the image in formed, exact value of L can not be solved for and it is estimated by a camera calibration program by finding the optimum solution.

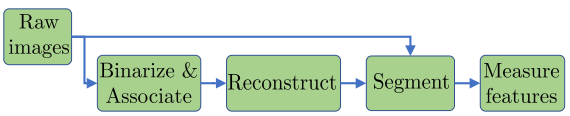

Figure 3.1: Flowchart of multi-insect tracking program

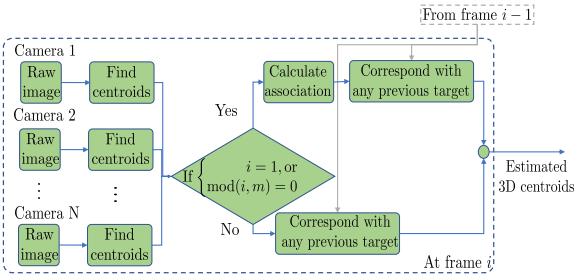

Figure 3.2: Insect association steps

The camera projection equation here is

$$\lambda \begin{bmatrix} a & b & 1 \end{bmatrix}^T = L_{3\times 4} \begin{bmatrix} X & Y & Z & 1 \end{bmatrix}^T \tag{3.1}$$

where, L is the DLT matrix,a, b are pixel co-ordinates of a point in 2-D image,λ is scaling factor,(X, Y, Z) is 3-D point in space.

We used the (Svoboda et al., 2005) calibration routine to compute L. This routine requires a single laser pointer to be entered into the test arena such that the multiple cameras may distinguish one 3D points in several 2D image points. Using this information the program gives an estimate of L. The output L needs to be adjusted if we choose to shift to another global reference frame of choice with preferred origin and orientation.

3.2 Insect Association

This part of the tracker identifies one individual insect in different 2D camera views as shown in Figure. 3.2. Multiple insect centroids are identified in each view by subtracting the average background calculated from the images in each frame to detect the blobs.

Association is done by testing 3D points visible in the greatest number of cameras against a reprojection threshold as in the real-time (Straw et al., 2011), which is implemented in a MATLAB adaptation. This implementation is adapted for post-

processing by including a capability to use different cameras for reconstruction and association tasks, subject to the limitation of visibility in more than 2 cameras. In this implementation we also allowed to assign multiple object ids to a single blob with nearest neighbour assignment corresponding to the case where the insect cover each other in a camera view. This does not create a major problem if they can be separated in any other camera views because eventually the reconstruction routine can separate them in 3D.

For association every possible combination of triangulated 3D points from 2D centroids in multiple views is tested. Any 3D point with visible in greatest number of cameras with a re-projection error less than a chosen threshold is considered a valid association point. In a N camera system,let $m_n \in [1, 2, \cdots, j]$ when there are j insects present in n^{th} camera view.$C_n^m = \begin{bmatrix} a_n^m & b_n^m \end{bmatrix}$ refers to m^{th} centroid in n^{th} camera view,where a, b refers to 2D pixel co-ordinates of image. A test combination of detected centroids, $T_{n\times 2} = \begin{bmatrix} C_1^{m_1} & C_2^{m_2} & \cdots & C_n^{m_n} \end{bmatrix}^T$ where,$2 \leq n \leq N$,is defined valid if every row i of the corresponding re-projection error vector δ has $\max_{i=1,2,\ldots,N} \delta_i < \eta$. where,

$$
\begin{aligned}
P &= \ solve3D(T) \\
T' &= \ project(P) \\
\xi &= T - T' \\
\delta_i &= \|\xi_i\|_2
\end{aligned}
$$

Here,*project* uses camera projection equations (3.1) with 3D points to find the projected point in 2D. *solve3D* uses camera projection with 2D points in available cameras to a solve for a 3D point optimum in a least square sense.

With all valid combinations which are visible in the most number of cameras the

association set $A = \{T^1, T^2, ...T^j\}$ is computed where the frame contains maximum of j insects. The implementation supports arbitrary number of cameras with the flexibility to choose a subset of cameras if required for association and can keep track of insects visible in at least 2 cameras. After association matrix is computed, it is matched with any existing targets by minimizing target to target distance.Since η is a chosen variable, tuned specifically to the camera setup used.

3.3 Insect Reconstruction

The 3D space in consideration can be discretized into volume pixels or voxels. With a valid associated centroid list available at each time step, we take every element in association set A to generate estimated centroid $P^i = solve3D(T^i)$. This point is then projected into voxel space,and a predefined scaler length, l obtained from the average size of a honey bee is used to define a search space such that P^i lies in the centroid of the cube with length l. For each point in this cubic search space, a point P^k is registered as an insect voxel if it can be projected back on the insect blob in a preset number of camera views. In our implementation we kept voxels which could be projected back on a binarized insect image in at least 3 views based on visibility in the cameras.

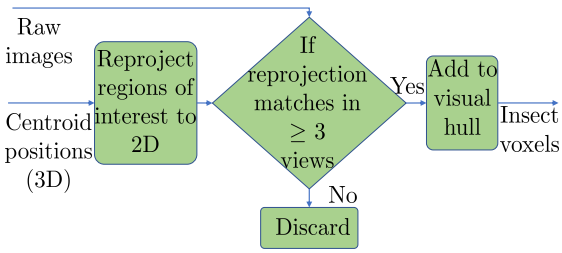

Figure 3.3: Insect reconstruction steps

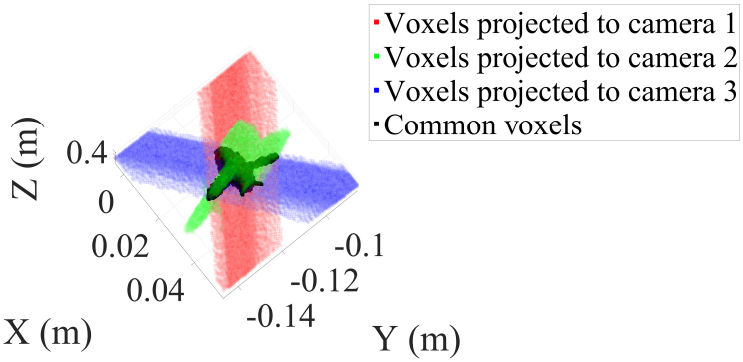

Figure 3.4: Insect is reconstructed by taking the common voxels in search area that could be projected back to insect pixels in the camera images

3.4 Insect Segmentation

Segmentation refers to dividing the insect voxels into body and wing voxels. At first intensities of the insect pixels in each 2D view is used to do a preliminary segmentation which is refined in subsequent steps. In each view, the 2D insect pixels can be clustered into two different groups where the darker and lighter pixels refer to the body and wing pixels. The histogram obtained from the pixel intensities as shown in Figure 3.6 is used to estimate the probability density of intensity using a kernel density estimator(Hill, 1985). The probability density function generally have two peaks and the value of normalized intensity at the minima between two peaks of the distribution is used as a segmentation threshold value to separate out wing pixel from body pixels. A voxel is assigned as a wing voxel if any of the views identify it as a wing, because the body is visible through the transparent wing. In this step, the border voxels will be misidentified as wing voxels and we further refine it by removing any wing pixel

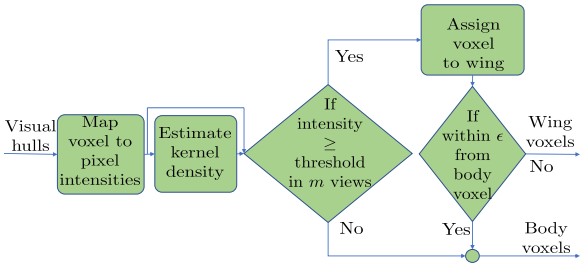

Figure 3.5: Segmentation to body/wings steps

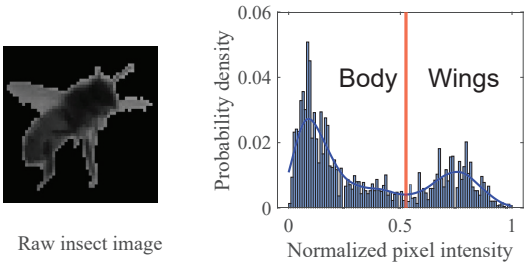

Figure 3.6: 2D pixels on each insect body can be segmented to body and wing based on their intensity

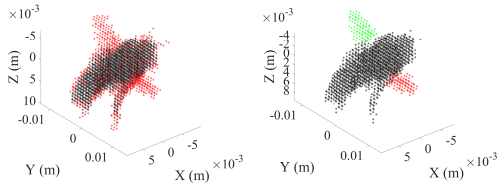

Figure 3.7: Purely intensity based segmentation leaves ambiguous voxels close to the boundary of body voxels. Wing voxels withib ϵ from body are thrown out

that is too close to the body and we also remove isolated disconnected wing voxels if any. After this step, a k-means segmentation with k=2 separates out 2 wings as in Figure 3.7

3.5 Calculating insect features

Each insect is modeled as a 12-dof system with position of body center of mass, orientations of body and 2 wings.

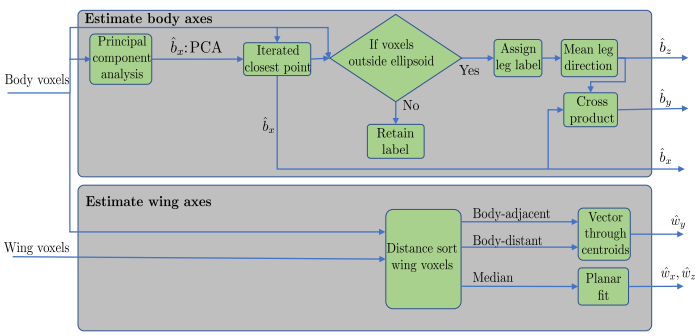

Figure 3.8: Insect feature calculation steps

Type	Variable	Description
Axes/Directions	$\{\hat{\boldsymbol{x}}, \hat{\boldsymbol{y}}, \hat{\boldsymbol{z}}\}$	Global frame axes,$\mathcal{G}$
	$\{\hat{\boldsymbol{s}}_{\boldsymbol{x}}, \hat{\boldsymbol{s}}_{\boldsymbol{y}}, \hat{\boldsymbol{s}}_{\boldsymbol{z}}\}$	Stability frame axes,$\mathcal{S}$
	$\{\hat{\boldsymbol{b}}_{\boldsymbol{x}}, \hat{\boldsymbol{b}}_{\boldsymbol{y}}, \hat{\boldsymbol{b}}_{\boldsymbol{z}}\}$	Body frame axes,$\mathcal{B}$
	$\{\hat{\boldsymbol{w}}_{\boldsymbol{x}}, \hat{\boldsymbol{w}}_{\boldsymbol{y}}, \hat{\boldsymbol{w}}_{\boldsymbol{z}}\}_{R/L}$	Right/Left wing frame axes,$\mathcal{W}$
	$\boldsymbol{r}_l$	Average leg direction
Orientation	θ_b	Body pitch angle
Velocities and angular rates	$\boldsymbol{v}^G$	Body velocity
	$\boldsymbol{\omega}^B$	Body angular velocity
	u, v, w	Body translational rates $\boldsymbol{v}^G$ in $\mathcal{S}$ coordinates
	p, q, r	Body rotational rates $\boldsymbol{\omega}^B$ in $\mathcal{S}$ coordinates
Wing parameters	$\phi_{R,L}$	Wing stroke angle
	$\psi_{R,L}$	Wing elevation angle
	$\beta_{R,L}$	Stroke plane angle
Forces and moments	X, Y, Z	Forces expressed in stability axis,$\mathcal{S}$
	L, M, N	Moments expressed in stability axis,$\mathcal{S}$

Table 3.1: Notations used for defining insect pose

3.5.1 Insect parameters definitions and notation

Insect body parameters used in this paper are described in Table 3.1 and Figure 3.11,3.9

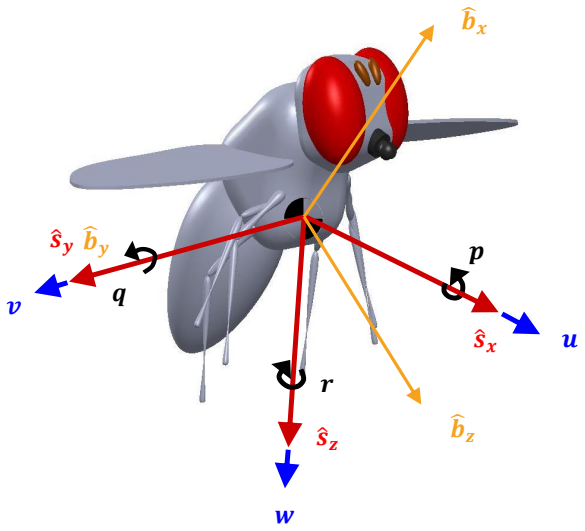

Figure 3.9: Body and stability axes to define insect orientation

3.5.2 Identifying body frame

The body fixed frame aligns with head-right-down, $\hat{\boldsymbol{b}}_{\boldsymbol{x}}, \hat{\boldsymbol{b}}_{\boldsymbol{y}}, \hat{\boldsymbol{b}}_{\boldsymbol{z}}$ respectively. The roll angle is the most difficult one to identify in insect due to its nearly cylindrical shape (Fontaine et al., 2009). However using legs as a reference can improve the determination of roll angle. We assumed that the insect legs can only rotate about $\hat{\boldsymbol{b}}_{\boldsymbol{y}}$ and used the leg direction to detect roll angle. For doing this we fit a ellipsoid with Iterated Closest Point (ICP) (Chen and Medioni, 1992) algorithm to the body voxel cloud which computes a rotation matrix necessary to minimize point to point distance in two point clouds. We initialize the ellipsoid major axis overlapping with the first principal component of body voxels. We assume, any voxels lying outside the ellipsoid

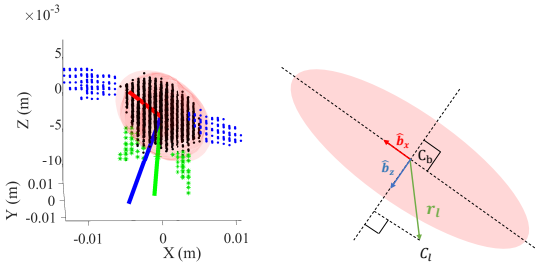

(a) Leg detection (b) $\hat{\boldsymbol{b}}_{\boldsymbol{z}}$ determination

Figure 3.10: Reconstructed legs are used for determination of $\hat{\boldsymbol{b}}_{\boldsymbol{z}}$

should refer to the leg voxels. The rotated ellipsoid major axis taken as $\hat{\boldsymbol{b}}_{\boldsymbol{x}}$. Then the centroid of leg voxels is used to identify $\hat{\boldsymbol{b}}_{\boldsymbol{z}}$. If, $\boldsymbol{r_l}$= vector in the body centroid to leg centroid direction expressed in global axis, $\hat{\boldsymbol{b}_{\boldsymbol{z}}}$ can be obtained by,

$$\hat{\boldsymbol{b}}_{\boldsymbol{z}} = \frac{\boldsymbol{b_z}}{|\boldsymbol{b_z}|}, \qquad \boldsymbol{b_z} = \boldsymbol{r_l} - \frac{\boldsymbol{r_l} \cdot \hat{\boldsymbol{b}}_{\boldsymbol{x}}}{|\boldsymbol{r_l}|}$$

If legs can not be reconstructed sufficiently good enough due to poor visibility, we impose the roll constraints as used in Fontaine et al. (2009) to determine roll axis which assumes symmetry of wings about the transverse plane of body.

3.5.2.1 Identifying wing frame

The wing frames are initially aligned with the body frame such that right wing span,$\hat{\boldsymbol{w}}_{\boldsymbol{y}} = \hat{\boldsymbol{b}}_{\boldsymbol{y}}$ and normal $\hat{\boldsymbol{w}}_{\boldsymbol{z}} = \hat{\boldsymbol{b}}_{\boldsymbol{z}}$. In each time step the major wing span direction $\hat{\boldsymbol{w}}_{\boldsymbol{y}}$ is determined by taking the connecting vector between centroids of 20% closest (hinge) and furthest (tip) wing voxels to the body. The normal to the wing,$\hat{\boldsymbol{w}}_{\boldsymbol{z}}$ is determined by the normal of the plane fitted through the remaining 60% wing voxels in the middle.

3.5.3 Determination of wingbeat frequency and amplitude

The wing angles are defined as the rotations needed to transform the body frame to a wing frame in each time instant. The right wing euler 3-1-2 angles ϕ_R, ψ_R, α_R were projected to get in plane motion with the following equation.

$$\gamma_R = -\phi_R \cos\beta_R + \psi_R \sin\beta_R$$

Here β_R refers to the average stroke plane angle (Figure 3.11) which is determined by linear fitting of ϕ_R and ψ_R over a single wingbeat length. The fast Fourier transform of signal γ_R is then taken to obtain peak amplitude,Φ and peak frequency,f.

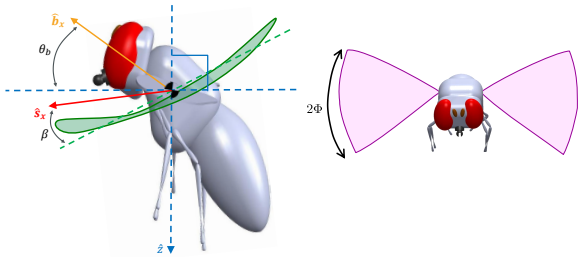

Figure 3.11: Wingbeat amplitude and body pitch angle definitions

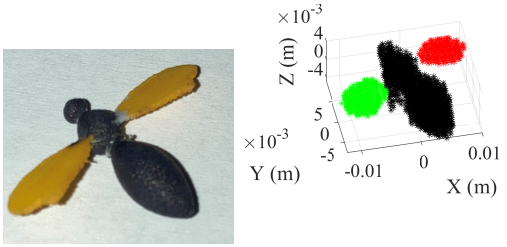

(a) Reference insect (b) Reconstructed hull

Figure 3.12: Reconstruction of a reference model insect

3.5.3.1 Determination of body pitch angle

The body pitch angle is defined by the complementary angle of the angle between global vertical ($-\hat{\boldsymbol{z}}$) axis and body roll axis ($\hat{\boldsymbol{b}}_{\boldsymbol{x}}$) according to Figure 3.11.

3.6 Validation

When calibrating the camera the projection matrices were taken which give less than 0.5 pixels mean reprojection error in order to minimize reconstruction error.

In order to test the tracker performance the wing angles of a 3D printed insect was determined. In 500 frames the tracker determined the 3-1-2 euler angles with the reported error in Table 3.2.

Wing	Mean Error, °	Std. Dev., °
Left	(-2.6, 0.6, 6.3)	(1.0, 1.3, 0.9)
Right	(-5.6, -3.4, 5.4)	(1.3, 0.8, 1.4)

Table 3.2: Error in Euler (3,1,2) wing angle estimation for 3D printed insect

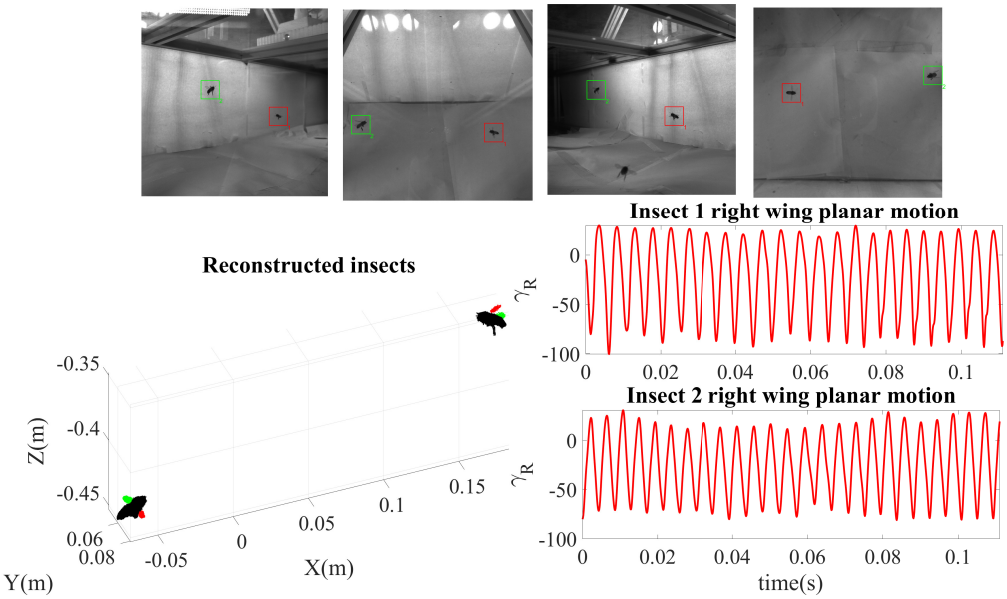

Figure 3.13: Example of tracker output

3.7 Example output

An example of the tracker working is shown in 3.13.

CHAPTER IV

ETHANOL EXPOSED HONEY BEE FLIGHT

The goal of this study is to test our multi-insect tracker on free flights of honeybees and chemically exposed bees and examine the variables that may have been influenced by ethanol exposure. This study is the first one testing flight behaviours with chemically exposed insects and works as a foundation to more detail study on flight behaviour.

4.1 Experimental Setup

A T-shaped tunnel was built with one of it ends attached to a beehive of *Apis mellifera* residents and two others for exiting freely from the setup. 4 Photron high speed cameras were set up to film the intersection of the T-joint at 9000 Hz.

4.2 Preparation of chemically-exposed insects

Captured insects were anesthetized by storage below freezing for 3 minutes, and restrained in a harness made from a modified micro centrifuge tube. The insects were then fed sucrose solution until no proboscis extension reflex was present and then let rest for approximately 24 hours at 72° F. This preparation ensured a consistent metabolic state at the beginning of experiments. In ethanol-exposure experiments, insects were then fed ethanol solution, kept for 15 minutes, and added to the flight test chamber. Each insect was removed from the test arena within 30 minutes of releasing to the test chamber to ensure flight is recorded under chemical influence. In this paper two types of insect flights are discussed.

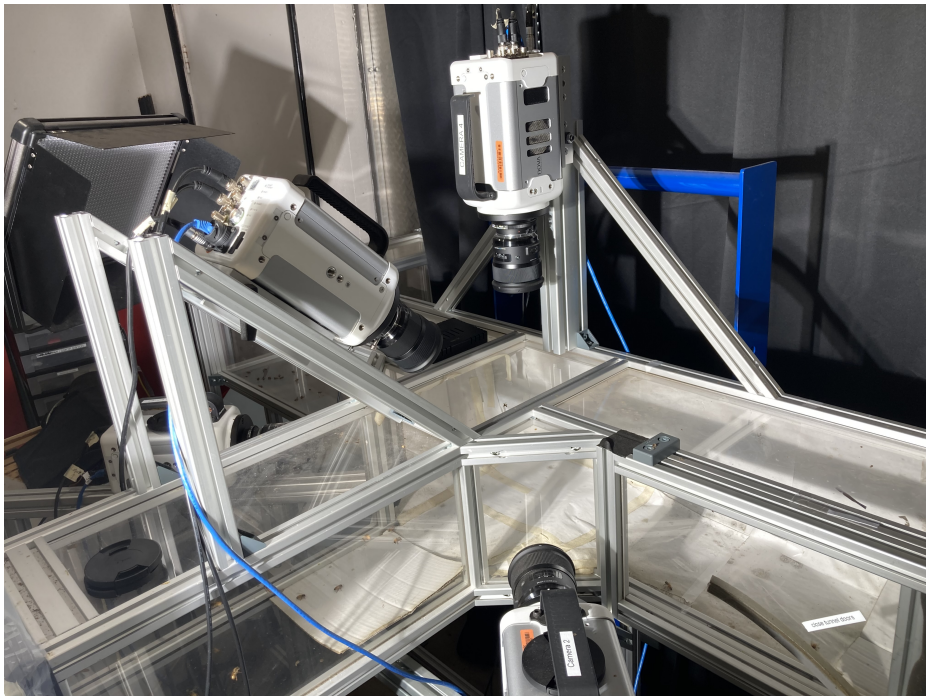

Figure 4.1: Tunnel setup attached to a beehive with camera setup to film the intersection

Figure 4.2: Restrained honeybees for chemical preparation.

Solution	50% Sucrose	95% C_2H_6O	H_2O, distilled
0%	40ml	0 ml	60 ml
1%	40ml	1.05 ml	58.95 ml
2.5%	40ml	2.63 ml	57.37 ml
5%	40ml	5.26 ml	54.74 ml

Table 4.1: Ethanol preparation recipes

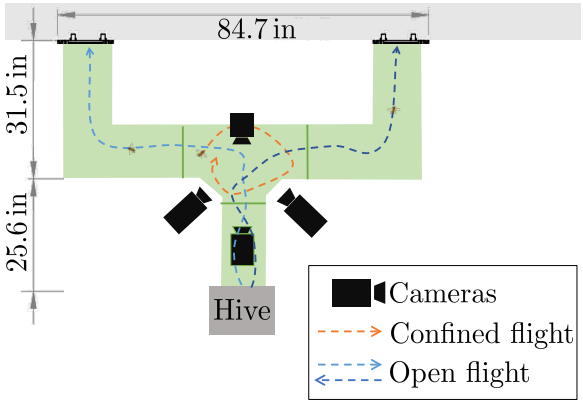

Figure 4.3: Insects fly through the whole tunnel in open tunnel experiments. In confined flights the intersection in confined by adding partitions.

4.3 Open flights

Honey bee workers were filmed when they were moving freely through the tunnel. The data was collected between 4 pm to 5 pm when the primary activity was foragers returning to the hive. In these trials multiple of them crossed the test section showing wide range of maneuvers. 60 flight sequences were analyzed for this study.

4.4 Ethanol exposed flights

In this experiment we recorded flights bees exposed with control 0%,1% and 2.5% and 5% ethyl-alcohol. These experiments were done in a confined environment in the tunnel by blocking exits. A total of 33 trials were collected(9 of 0%, 8 of 1%, 8 of 2.5%, 8 of 5%).

4.5 Parameters considered

For this study, the state variables in each flight sequence are represented by 15 (scalar) variables. For a time history over $[0, T_r]$, where T_r is the time length recorded, time t was discretized as $t_i, i = 1, 2, 3..., n$ at a constant sample frequency, and the mean

value of a variable $h(t)$ measured the flight sequence was calculated as

$$\bar{h} := \frac{1}{n}\sum_{i=1}^{n} h(t_i), \quad t_i \in [0, T_r] \tag{4.1}$$

and the maximum value is defined as

$$h_{max} := \max_{t\in[0,T_r]}[h(t)]. \tag{4.2}$$

Each flight sequence was characterized by 15 scalar values as shown in Table 4.2. We define the set of these scalars as B.

Notation	Description
f	Peak wingbeat frequency
Φ	Peak wingbeat amplitude
$\bar{\theta_b}$	Mean body pitch angle
$\|\bar{u}\|$	Mean absolute forward speed
$\|\bar{v}\|$	Mean absolute sideways speed
$\|\bar{w}\|$	Mean absolute heave speed
$\|\bar{p}\|$	Mean absolute roll rate
$\|\bar{q}\|$	Mean absolute pitch rate
$\|\bar{r}\|$	Mean absolute yaw rate
$\|u\|_{max}$	Maximum absolute forward speed
$\|v\|_{max}$	Maximum absolute sideways speed
$\|w\|_{max}$	Maximum absolute heave speed
$\|p\|_{max}$	Maximum absolute roll rate
$\|q\|_{max}$	Maximum absolute pitch rate
$\|r\|_{max}$	Maximum absolute yaw rate

Table 4.2: Characterizing variables in flight sequence

For each,$s \in B$ we consider population-wise mean and standard deviation. The mean value of population of a variable is defined as

$$\mu(s) := \frac{1}{n}\sum_{i=1}^{n} s_i \tag{4.3}$$

where, n is the number of flight sequences recorded for the concerned category(Open,0%,.. etc).

The standard deviation of population of a variable is defined as

$$\sigma(s) := (\frac{1}{n}\sum_{i=1}^{n}(s_i - \mu(s))^2)^{1/2} \tag{4.4}$$

4.6 Analysis tools and methods

In order to find significant variables we did binary statistical analyses by dividing the data in groups (G_0, G_1, G_2). The following cases were considered:

- Case-1: G_0(Open) Vs $G_1(0\%)$, to find significant changes between open and confined insect flights.
- Case-2: $G_1(0\%)$ Vs $G_2((1\%, 2.5\%, 5\%))$, to find significant changes between exposed/unexposed insect flights.

The statistical tools we considered are one-way Analysis of Variance(ANOVA), Cohen's d test, and Welch's t-test.

ANOVA and Welch's t-test checks the null hypothesis that two populations have equal means for some variable. We checked this hypothesis for each,$s \in B$ where, the null hypotheses are,

- Case-1: $\mu_{G_0}(s) = \mu_{G_1}(s)$
- Case-2: $\mu_{G_1}(s) = \mu_{G_2}(s)$

The simple one way ANOVA works on the assumptions that the response variable residuals are normally distributed and the variances of populations are equal. The Welch's t-test does not require the assumption of equal variance and more applicable when the sample sizes are not equal. The p-values provide us the probability of the null-hypothesis being true. Cohen's d effect size shows the shift of $\mu(s)$ in terms of pooled standard deviation. We apply these two tests on the dataset having sample points $(G_0(60), G_1(9), G_2(24))$.

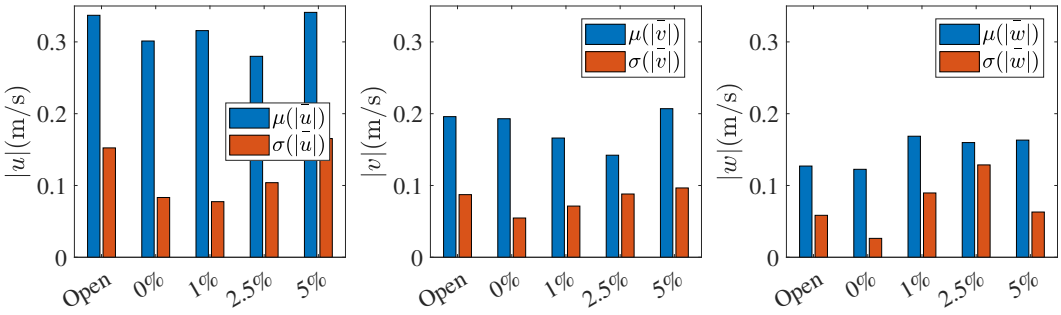

(a) $|\bar{u}|$ (b) $|\bar{v}|$ (c) $|\bar{w}|$

Figure 4.4: Mean absolute velocity statistics of population

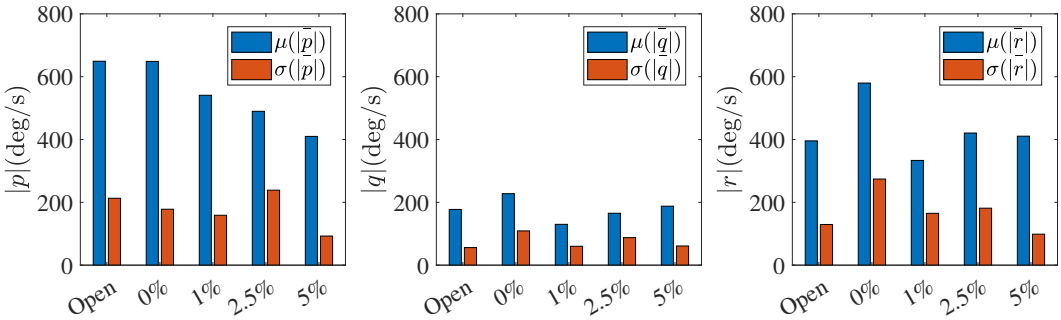

(a) $|\bar{p}|$ (b) $|\bar{q}|$ (c) $|\bar{r}|$

Figure 4.5: Mean absolute body rate statistics of population

4.7 Results and Discussion

The simple one way Anova works on the assumptions that the response variable residuals are normally distributed and the variances of populations are equal. From the limited set amount of data points we have $(G_0(60), G_1(9), G_2(24))$ if we assume those conditions to be true then, for case-1, observing the p-values in Table 4.3 and choosing $(p < 0.05)$ we observe the ANOVA test detects $|\bar{r}|, \bar{\theta}_b, \Phi, |q|_{max}, |\bar{q}|$ variables have some significant impacts. The closed environment insects tend to fly at a greater pitch angle as seen in Figure 4.9. As they have walls to land on their average pitch angle is higher. However having a greater pitch angle changes the aerodynamics of flight and so experiments in closed environment might not be a good replication for studying flight behaviour of free flights.

In case-2,when comparing ethanol exposed and unexposed From table 4.4 the

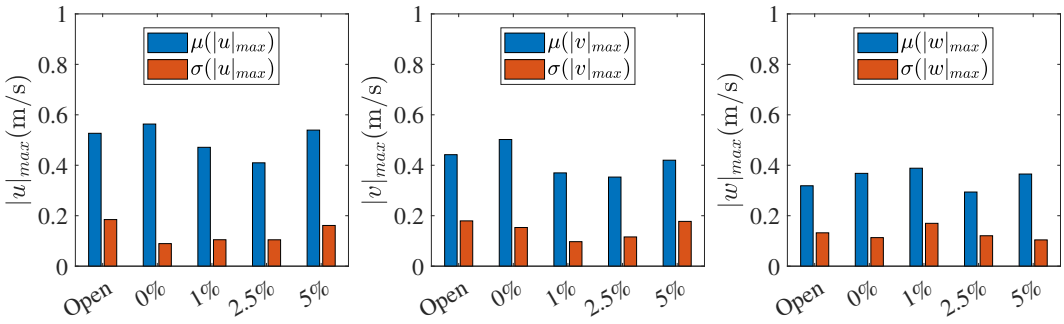

(a) $|u|_{max}$ (b) $|v|_{max}$ (c) $|w|_{max}$

Figure 4.6: Maximum absolute velocity statistics of population

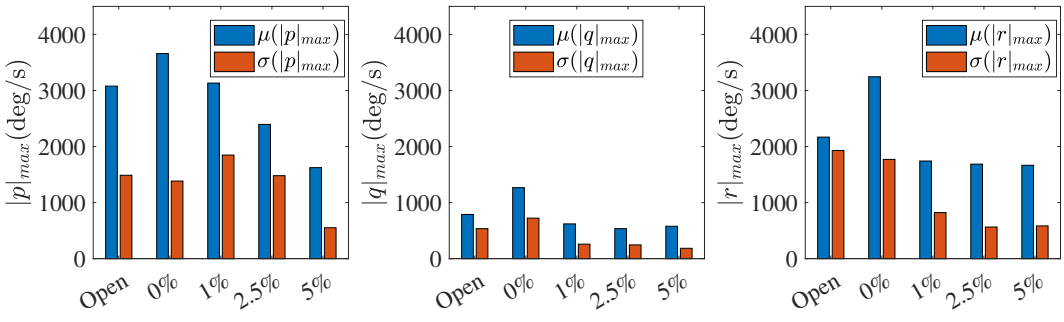

(a) $|p|_{max}$ (b) $|q|_{max}$ (c) $|r|_{max}$

Figure 4.7: Maximum absolute body rate statistics of population

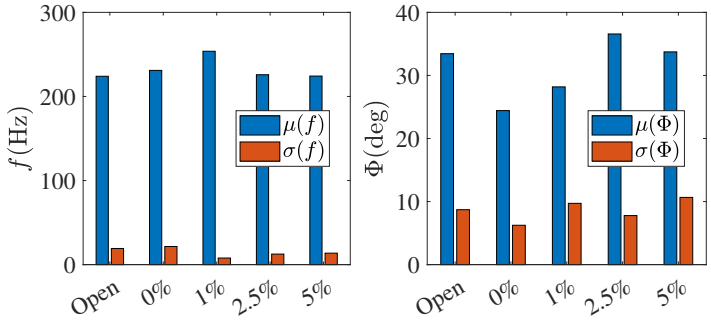

(a) f (b) Φ

Figure 4.8: Wing motion statistics of population

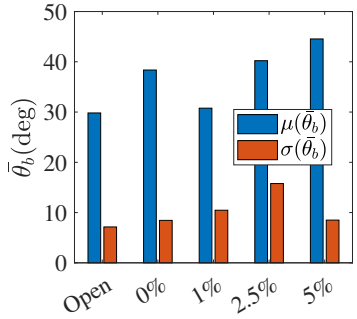

Figure 4.9: Mean body pitch angle, $\bar{\theta}_b$ statistics of population

$\mu(.)$	p-value(ANOVA)	d	p-value(Welch's t)
$\bar{\lvert r\rvert}$	0.0014	1.1944	0.0807
$\bar{\theta_b}$	0.0017	1.1688	0.0166
Φ	0.0039	-1.0675	0.0021
$\lvert q\rvert_{max}$	0.0200	0.8522	0.0876
$\bar{\lvert q\rvert}$	0.0335	0.7760	0.2104
$\lvert r\rvert_{max}$	0.1196	0.5636	0.1207
$\lvert p\rvert_{max}$	0.2744	0.3939	0.2695
$\lvert w\rvert_{max}$	0.2941	0.3780	0.2589
f	0.3196	0.3584	0.3795
$\lvert v\rvert_{max}$	0.3442	0.3406	0.3056
$\bar{\lvert u\rvert}$	0.4945	-0.2455	0.3070
$\lvert u\rvert_{max}$	0.5622	0.2082	0.3480
$\bar{\lvert w\rvert}$	0.8202	-0.0816	0.6989
$\bar{\lvert v\rvert}$	0.9230	-0.0347	0.8937
$\bar{\lvert p\rvert}$	0.9940	-0.0027	0.9932

Table 4.3: Open vs 0% comparison. Table is sorted by p-value(ANOVA)

strongest effects ($p < 0.01$) are seen with $|q|_{max}$,$|r|_{max}$. This suggests a potential effect in flight stabilization characteristics. The unexposed bee can reach higher $|p|_{max}, |q|_{max}, |r|_{max}$ as seen in Figure 4.7a,4.7b,4.7c suggesting that body rate regulation can be affected under the influence of ethanol.The all other mean body rates are also affected ($p < 0.05$) showing the possibility of affected flight stabilization reflex.Increase in Φ is also observed in Figure 4.8b suggesting a wing motion change as well.

The Welch's t-test does not require the assumption of equal variance and more applicable when the sample sizes are not equal. With this looser assumption we can still find that in Welch's t-test ($p < 0.05$) the most impacted variables for Case-1, are $\bar{\theta_b}, \Phi$ which agrees with the previous observation.Both of these variables also show high effect size ($|d| > 0.8$). For Case-2, the Welch's test show $|v|_{max}$ with $(p = 0.056), \bar{|r|}$ with $(p = 0.07)$ may not have been significantly changed and $|u|_{max}$ might have changed which was not captured in ANOVA test.However, they both show that $|q|_{max}, |r|_{max}, \bar{|p|}, |p|_{max}, \Phi$ has significant changes. We get large effect size for each of them ($|d| > 0.8$) which suggest they are handling lower body rates with higher wingbeat amplitude.

$\mu(.)$	p-value(ANOVA)	d	p-value(Welch's t)
$\|q\|_{max}$	0.0002	-1.6602	0.0214
$\|r\|_{max}$	0.0007	-1.4679	0.0313
$\|\bar{r}\|$	0.0152	-1.0045	0.0755
$\|\bar{p}\|$	0.0201	-0.9579	0.0288
Φ	0.0225	0.9391	0.0077
$\|v\|_{max}$	0.0317	-0.8793	0.0566
$\|p\|_{max}$	0.0324	-0.8754	0.0350
$\|\bar{q}\|$	0.0490	-0.8009	0.1184
$\|u\|_{max}$	0.0702	-0.7331	0.0360
$\|\bar{w}\|$	0.2039	0.5073	0.0580
$\|\bar{v}\|$	0.5001	-0.2667	0.4118
f	0.6262	0.1923	0.6611
$\|w\|_{max}$	0.7138	-0.1447	0.6930
$\|\bar{u}\|$	0.8009	0.0994	0.7683
$\bar{\theta_b}$	0.9747	0.0125	0.9696

Table 4.4: Closed exposed(1%,2.5%,5%) vs unexposed(0%) comparison. Table is sorted by p-value(ANOVA)

All these statistical inferences show that there is some kind of effect is in place without giving us the explicit reasons behind them. We also did not account for inter-dependence of variables.These questions can be addressed in future studies.

CHAPTER V

SYSTEM IDENTIFICATION APPROACH IN MULTI-AGENT FLIGHT

5.1 Introduction

System identification is a mature field today undergoing continuous improvements. It focuses on extracting the underlying relation between input and output signals. Insect flying near neighbours show interaction among them enabling them to perform maneuvers to avoid collision, speed matching etc. In order to understand these behaviours quantitivly some mechanism is needed to analyze the flight data. In this section we build a simple framework which can be used to analyse multi-insect data to learn about their interaction rules. With our tracker we have access to the control inputs of the insect to control their flight. In this implementation we mainly focus on collision avoidance though it can be modified to analyze other behaviours too. For simplicity we work with existing linearized insect motion model. With available time history of insect wing inputs, a time domain least square regression identification example is shown.

5.2 Linearized Lateral Flight Dynamics of Insects

An insect flying straight forward with constant speed maintains it's stability in lateral direction. For maintaining stability while flying near neighbours it needs distance information from the neighbour to adjust its wing motion to slightly change path and avoid collision. Dipteran insect motion about hover has been formulated previously in (Faruque and Humbert, 2010a) and (Faruque and Humbert, 2010b) for stability

along their longitudinal and lateral directions. The lateral directional stability model describes an insect flying at a nearly constant speed and the necessary wing inputs to maintain stability at the trim condition.

body sideways velocity in expressed in stability axis, v

body roll rate in stability axis,p

body roll angle in stability frame,ϕ

body yaw rate in stability frame,r

The state vector here,$x = \begin{bmatrix} v & p & \phi & r \end{bmatrix}^T$

The control inputs that control this motion are shown as in Fig,5.1,

Differential stroke amplitude,$\phi_d = \frac{1}{2}(\phi_r - \phi_l)$

Differential stroke amplitude,$\beta_d = \frac{1}{2}(\beta_r - \beta_l)$

Control input, $u = \begin{bmatrix} \phi_d & \beta_d \end{bmatrix}^T$

The linearized state space representation of the system is given by,

$$\dot{x} = Ax + Bu \tag{5.1}$$

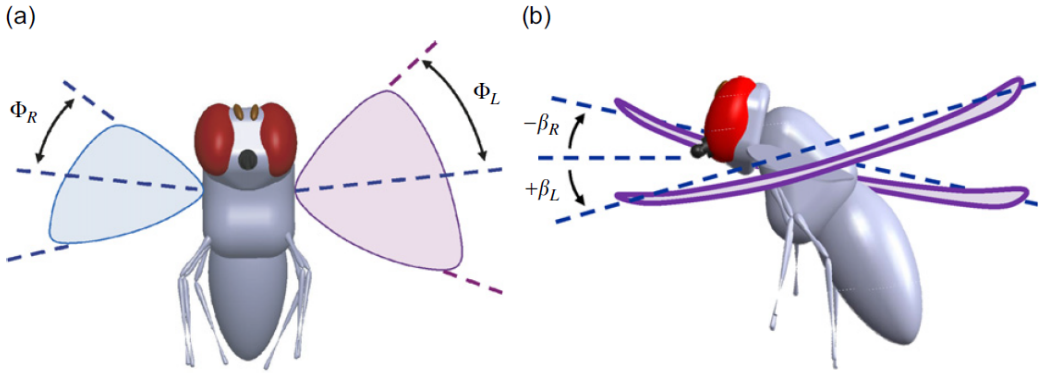

Figure 5.1: Lateral directional inputs

Where,

$$A = \begin{bmatrix} Y_v & 0 & g & 0 \\ L'_v & L'_p & 0 & L'_r \\ 0 & 1 & 0 & 0 \\ N'_v & N'_p & 0 & N'_r \end{bmatrix}, B = \begin{bmatrix} Y_{\phi_d} & 0 \\ L_{\phi_d} & 0 \\ 0 & 0 \\ 0 & N_{\beta_d} \end{bmatrix}$$

X, Y, Z and L, M, N are forces and moments respectively and $[.]_x$ represents partial derivative with respect to x.

This model is ideal when a insect is flying straightly forward attempts to correct the mentioned states to stay stable. When solitary flight is considered we can assume that the insect uses its states as feedback to stabilize the motion.

$$u = -K_{fb}x \tag{5.2}$$

When it is not flying alone we can assume that it is also sensing some external signal v that also influences its control inputs.

$$u = -K_{fb}x + K_{ext}v \tag{5.3}$$

The exact signal v an insect is using may not be determined clearly, but we can make synthetic signals which is applicable to the specific behavior we are observing and try to estimate how good that synthetic signal explains the data using system identification. The gain K_{ext} takes the synthetic signal to influence wing input in order to control motion. In this example we will derive a potential synthetic signal that might be used by the insect to show collision avoidance mechanism.

5.3 Example design of a synthetic signal

As we are trying to understand collision avoidance mechanism we call this synthetic function as 'social distancing function'.It needs to have some inherent properties to

show collision avoidance. Firstly, it should decay with increased distance between neighbours so that if a neighbour is far away the signal needs to go to zero. Secondly, it needs to contain the direction at which a neighbour is located so that the insect can avoid that direction. Thirdly, it should be able to take in account the effects when the insect is surrounded with multiple neighbours.

let,$\mathbf{r_a}$ be the position vector of the insect in consideration and $\mathbf{r_i}$ the position vector of the neighbour i in the global frame. We can define the function with magnitude, $e^{-K_s\|\mathbf{r_i}-\mathbf{r_a}\|}$ in the direction $\mathbf{r_i}-\mathbf{r_a}$,

$$\boldsymbol{d}_{\mathrm{g}} = e^{-K_s\|\boldsymbol{r_i}-\boldsymbol{r_a}\|}\frac{\mathbf{r_i}-\mathbf{r_a}}{\|\mathbf{r_i}-\mathbf{r_a}\|} \tag{5.4}$$

Here K_s is a constant tuning the strength of the signal depending on the distance to its neighbour.

The vector $\boldsymbol{d_g}$ is expressed in global frame co-ordinates. We reorient it to the stability frame of the insect so that $\boldsymbol{d} = \begin{bmatrix} d_x & d_y & d_z \end{bmatrix}^T$ represent the repulsion strength in the stability axes directions $\hat{\boldsymbol{s}}_{\boldsymbol{x}}, \hat{\boldsymbol{s}}_{\boldsymbol{y}}, \hat{\boldsymbol{s}}_{\boldsymbol{z}}$. If there are multiple agents we can add up their effects by choosing the synthetic signal as, $\boldsymbol{v} = \sum_{i=1}^{n} \boldsymbol{d_i}$, where there are total n neighbours.

5.4 Simulation

For simulation, We set the model of a typical insect in Faruque and Humbert (2010b) as the system,

$$\begin{bmatrix} \dot{v} \\ \dot{p} \\ \dot{\phi} \\ \dot{r} \end{bmatrix} = \begin{bmatrix} -9.69 & 0 & 9.81 & 0 \\ -9720.0 & -177 & 0 & -2.07 \\ 0 & 1 & 0 & 0 \\ -167.0 & 462.0 & 0 & -71.6 \end{bmatrix} \begin{bmatrix} v \\ p \\ \phi \\ r \end{bmatrix} + \begin{bmatrix} 8.24 & 0.0 \\ -12300 & 0 \\ 0 & 0 \\ 0 & -28100 \end{bmatrix} \begin{bmatrix} \phi_d \\ \beta_d \end{bmatrix}$$

The controller K_{ext} was chosen in such a way that collision avoidance can be observed. We set, $K_{ext} = \begin{bmatrix} 0.001 & -2.0 & 0.001 \\ 0.005 & 0.01 & 0.02 \end{bmatrix}$. The intuition behind this controller is that the insect must move in the opposite direction of an agent at its side. The $K_{ext,(1,2)} = -2$ term is multiplied the social distancing component in stability axis $\hat{s}_y$, and generates input to the ϕ_d which is the primary way to generate a sideways acceleration $\dot{v}$.

For simulation we set a forward speed $u = 0.1$m/s,and $x = \begin{bmatrix} 0 & 0 & 0 & 0 \end{bmatrix}^T$ as initial condition. The insect starts its journey from position $\begin{bmatrix} 5 & 6 & 7 \end{bmatrix}^T$ meter in global frame with its stability frame aligned with the global frame initially. Two stationary insects are put in $\begin{bmatrix} 5.045 & 6.01 & 7.0 \end{bmatrix}^T$ meter and $\begin{bmatrix} 5.28 & 6.023 & 7.003 \end{bmatrix}^T$ meter. K_s was set 50/m.A virtual state feedback controller,$K_{fb} = \begin{bmatrix} 0.0790 & 0.0014 & 0 & 0 \\ 0.0006 & -0.0016 & 0 & 0 \end{bmatrix}$ so that $A_{cl} = A - BK_{fb}$ is stable was assumed to be working.

The simulation was run for 4 seconds with a sampling rate of 100Hz.

The example simulation of path in Figure. 5.2 show how this controller lets the agent avoid collision with stationary agents.

5.5 Experiment with honey bee data

In this example flight, one bee was trying to follow another bee while avoiding collision. With the same structure described for the simulation we identified K_{fb} and K_{ext}. The linearization point in this trial was:

$v = -0.0328\text{m/s}, p = 1.4439\text{rad/s}, \phi = 0.0672\text{rad}, r = 1.0808\text{rad/s}$

The forward mean forward speed of the bee was, $u = 0.1694$m/s

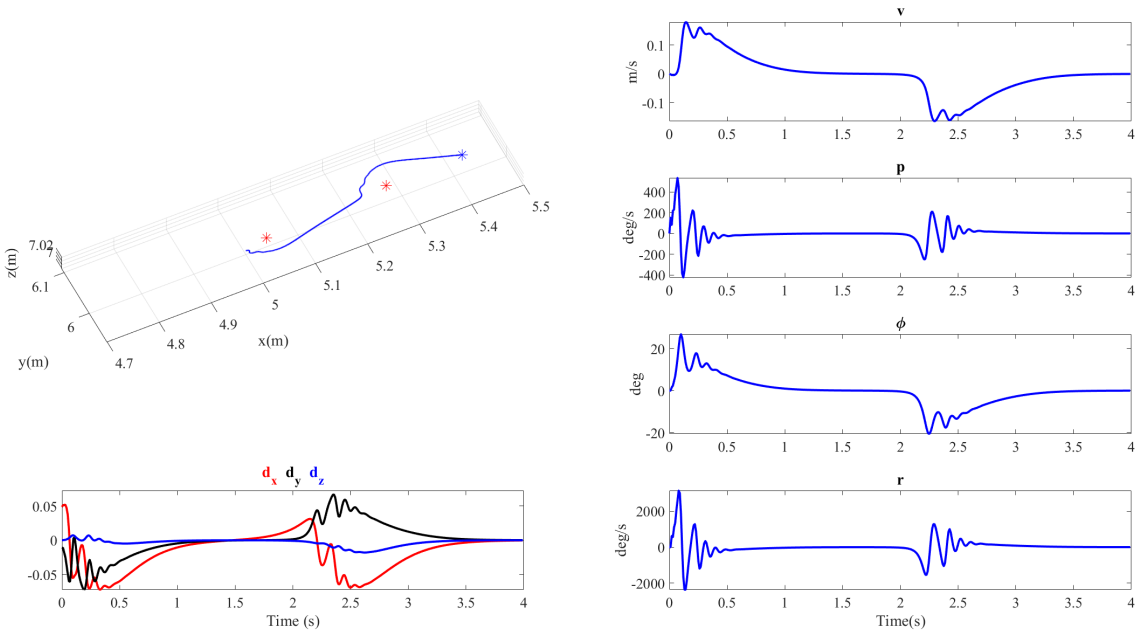

Figure 5.2: The target insect(blue) avoids two stationary agents (red) using the controller K_{ext}

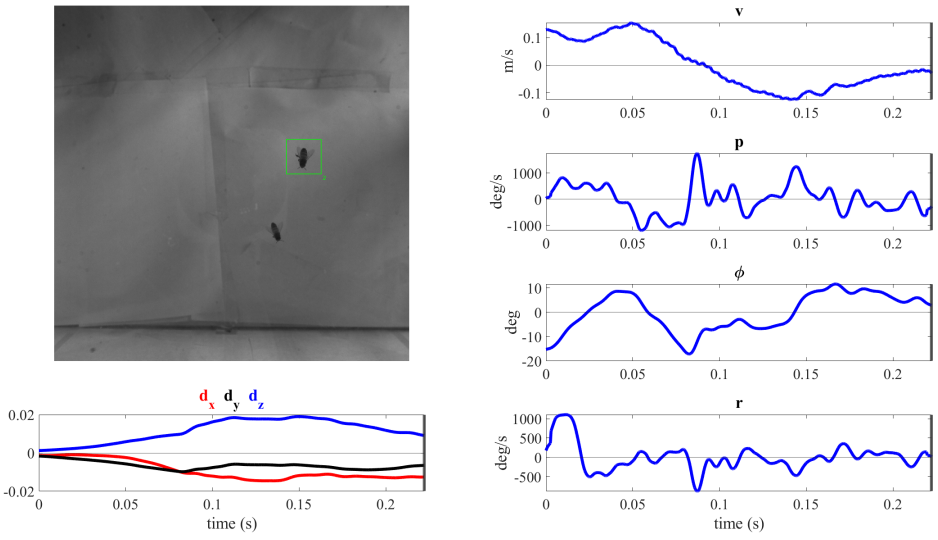

Figure 5.3: Example identification from real honey bee flight

5.6 System identification Method

From simulated and real experimental data we have the states time histories x, and control inputs u. We can use eq. 5.3 to define a linear regression problem

$$u = \begin{bmatrix} x & v \end{bmatrix} \begin{bmatrix} K_{fb} \\ K_{ext} \end{bmatrix}$$

$$\implies u = XK$$

$$\implies K = (X^T X)^{-1} X^T u$$

Where $X = \begin{bmatrix} x & v \end{bmatrix}$ and $K = \begin{bmatrix} K_{fb} & K_{ext} \end{bmatrix}^T$. Least square estimation was used to calculate K. The identification quality is assessed with Cramér-Rao lower bounds(**?**) which expresses a lower bound on the variance of unbiased estimators.

5.7 Results and Discussion

Controller	Identification Error	Cramér-Rao bounds
$K_{fb,id}$	$\begin{bmatrix} 0.0018 & 0.0000 & 0.0000 & 0.0000 \\ 0.0000 & -0.0000 & -0.0000 & 0.0000 \end{bmatrix}$	$10^{-27} \begin{bmatrix} 0.1179 & 0.0001 & 0.0036 & 0.0000 \\ 0.0004 & 0.0000 & 0.0000 & 0.0000 \end{bmatrix}$
$K_{ext,id}$	$\begin{bmatrix} -0.0000 & 0.0050 & -0.0000 \\ -0.0000 & -0.0000 & -0.0001 \end{bmatrix}$	$10^{-27} \begin{bmatrix} 0.0091 & 0.9505 & 0.4365 \\ 0.0000 & 0.0034 & 0.0016 \end{bmatrix}$

Table 5.1: Identified controller errors and Cramér-Rao bounds in simulation

Controller	Identified Values	Cramér-Rao bounds
$K_{fb,id}$	$\begin{bmatrix} -1.2224 & 0.0004 & 0.2897 & 0.0048 \\ 0.0788 & 0.0011 & 0.0658 & 0.0002 \end{bmatrix}$	$\begin{bmatrix} 0.0017 & 0.0000 & 0.0001 & 0.0000 \\ 0.0004 & 0.0000 & 0.0000 & 0.0000 \end{bmatrix}$
$K_{ext,id}$	$\begin{bmatrix} 12.1537 & -30.7815 & -13.3814 \\ -6.6250 & 4.1522 & -3.2751 \end{bmatrix}$	$\begin{bmatrix} 1.1895 & 1.8132 & 0.3545 \\ 0.2650 & 0.4040 & 0.0790 \end{bmatrix}$

Table 5.2: Identified controllers and Cramér-Rao bounds in experimental bee data

The simulated controllers can be identified with very low Cramér-Rao variance as shown in Table.5.1. The real experimental identification has Cramér-Rao variance several order of magnitudes higher than in simulation. The real insect does not follow

the assumed model perfectly and the linearization point was not exactly zero while the insect was showing the particular behaviour and therefore the identified parameters would have higher uncertainty as expected.

The formulation presented here can be adapted for other synthetic signals in order to study other types of group flight. As insect flights are diverse it is not always possible to find a idealized flight pattern like we did for a simulation.However a well designed synthetic signal may be able to extract valuable insights about the data. In chosen K_{ext} for simulation, we set $K_{ext(1,2)}$ to be the highest in magnitude as we wanted the insect to move sideways. In the identified K_{ext} in experiment we also see the highest magnitude in the $K_{ext(1,2)}$. In the simulation it is assumed that the forward speed remains constant through the trial which is very hardly achieved in real data. As the model is linearized, changes in the trim condition adds difficulty in identifying K_{ext} because K_{fb} may also change during that time. We can see these effects in real data observing the increased Cramér-Rao bounds as the fit quality degrades with these added uncertainties.

CHAPTER VI

CONCLUSION AND FUTURE WORK

In this work, a visual multi-insect kinematic tracker is constructed and it is applied to study ethanol exposed honey bees and an example system identification to study collision avoidance. This work builds the measurement tools necessary to study multi-insect with detailed kinematics. We see statistically significant changes in body rate and wingbeat amplitude behaviours when comparing ethanol exposed and unexposed insects. Also,open tunnel flights differed from closed tunnel flights with respect to body pitch angles suggesting that insect flight studies done in a closed environment may change it normal behaviour, A simple system identification example is worked out in simulation and real data to study collision avoidance group flight.

With the measurement tool developed in this thesis, further detailed studies of insect group interaction is possible. The ethanol exposure study tells us that the insect kinematics has changed and further studies with more sophisticated analyses tools may reveal the actual mechanisms and implications of it. The system identification examples worked out can be further developed into more mature frameworks to analyse inflight interaction between insects.

REFERENCES

Abdel-Aziz, Y., Karara, H., and Hauck, M. (2015). Direct linear transformation from comparator coordinates into object space coordinates in close-range photogrammetry*. *Photogrammetric Engineering & Remote Sensing*, 81(2):103–107.

Abramson, C. I., Craig, D. P. A., Varnon, C. A., and Wells, H. (2015). The effect of ethanol on reversal learning in honey bees (apis mellifera anatolica): Response inhibition in a social insect model. *Alcohol*, 49(3):245–258.

Abramson, C. I., Place, A. J., Aquino, I. S., and Fernandez, A. (2004a). Development of an ethanol model using social insects: Iv. influence of ethanol on the aggression of africanized honey bees (apis mellifera l.). *Psychological reports*, 94(3_suppl):1107–1115.

Abramson, C. I., Sanderson, C., Painter, J., Barnett, S., and Wells, H. (2005). Development of an ethanol model using social insects: V. honeybee foraging decisions under the influence of alcohol. *Alcohol*, 36(3):187–193.

Abramson, C. I., Sheridan, A., Donohue, D., Kandolf, A., Božič, J., Meyers, J. E., and Benbassat, D. (2004b). Development of an ethanol model using social insects: Iii. preferences for ethanol solutions. *Psychological reports*, 94(1):227–239.

Abramson, C. I., Stone, S. M., Ortez, R. A., Luccardi, A., Vann, K. L., Hanig, K. D., and Rice, J. (2000). The development of an ethanol model using social insects i: behavior studies of the honey bee (apis mellifera l.). *Alcoholism: Clinical and Experimental Research*, 24(8):1153–1166.

Ardekani, R., Biyani, A., Dalton, J. E., Saltz, J. B., Arbeitman, M. N., Tower, J., Nuzhdin, S., and Tavaré, S. (2013). Three-dimensional tracking and behaviour monitoring of multiple fruit flies. *Journal of The Royal Society Interface*, 10(78):20120547.

Bozic, J., DiCesare, J., Wells, H., and Abramson, C. I. (2007). Ethanol levels in honeybee hemolymph resulting from alcohol ingestion. *Alcohol*, 41(4):281–284.

Chen, Y. and Medioni, G. (1992). Object modelling by registration of multiple range images. *Image and vision computing*, 10(3):145–155.

Faruque, I. and Humbert, J. S. (2010a). Dipteran insect flight dynamics. part 1 longitudinal motion about hover. *Journal of theoretical biology*, 264(2):538–552.

Faruque, I. and Humbert, J. S. (2010b). Dipteran insect flight dynamics. part 2: lateral–directional motion about hover. *Journal of theoretical biology*, 265(3):306–313.

Fontaine, E. I., Zabala, F., Dickinson, M. H., and Burdick, J. W. (2009). Wing and body motion during flight initiation in drosophila revealed by automated visual tracking. *Journal of Experimental Biology*, 212(9):1307–1323.

Fry, S. N., Sayaman, R., and Dickinson, M. H. (2003). The aerodynamics of free-flight maneuvers in drosophila. *Science*, 300(5618):495–498.

Giannoni-Guzmán, M. A., Giray, T., Agosto-Rivera, J. L., Stevison, B. K., Freeman, B., Ricci, P., Brown, E. A., and Abramson, C. I. (2014). Ethanol-induced effects on sting extension response and punishment learning in the western honey bee (apis mellifera). *PloS one*, 9(7):e100894.

Gibson, J., May, T., and Wilks, A. V. (1981). Genetic variation at the alcohol dehydrogenase locus in drosophila melanogaster in relation to environmental variation: ethanol levels in breeding sites and allozyme frequencies. *Oecologia*, 51(2):191–198.

Grover, D., Tower, J., and Tavaré, S. (2008). O fly, where art thou? *Journal of the Royal Society Interface*, 5(27):1181–1191.

Hedrick, T. L. (2008). Software techniques for two- and three-dimensional kinematic measurements of biological and biomimetic systems. *Bioinspiration & Biomimetics*, 3(3):034001.

Hill, P. D. (1985). Kernel estimation of a distribution function. *Communications in Statistics - Theory and Methods*, 14(3):605–620.

Kostreski, N. I. (2012). *Automated kinematic extraction of wing and body motions of free flying diptera*. PhD thesis, University of Maryland.

Kuo, C.-H., Huang, C., and Nevatia, R. (2010). Multi-target tracking by on-line learned discriminative appearance models. In *2010 IEEE Computer Society Conference on Computer Vision and Pattern Recognition*, pages 685–692. IEEE.

Maze, I. S., Wright, G. A., and Mustard, J. A. (2006). Acute ethanol ingestion produces dose-dependent effects on motor behavior in the honey bee (apis mellifera). *Journal of insect physiology*, 52(11-12):1243–1253.

Mixson, T. A., Abramson, C. I., and Božič, J. (2010). The behavior and social communication of honey bees (apis mellifera carnica poll.) under the influence of alcohol. *Psychological reports*, 106(3):701–717.

Ristroph, L., Berman, G. J., Bergou, A. J., Wang, Z. J., and Cohen, I. (2009). Automated hull reconstruction motion tracking (hrmt) applied to sideways maneuvers of free-flying insects. *Journal of Experimental Biology*, 212(9):1324–1335.

Straw, A. D., Branson, K., Neumann, T. R., and Dickinson, M. H. (2011). Multi-camera real-time three-dimensional tracking of multiple flying animals. *Journal of The Royal Society Interface*, 8(56):395–409.

Svoboda, T., Martinec, D., and Pajdla, T. (2005). A convenient multicamera self-calibration for virtual environments. *Presence: Teleoperators & virtual environments*, 14(4):407–422.

Zhou, S. K., Chellappa, R., and Moghaddam, B. (2004). Visual tracking and recognition using appearance-adaptive models in particle filters. *IEEE Transactions on Image Processing*, 13(11):1491–1506.

VITA

Ishriak Ahmed

Candidate for the Degree of

Master of Science

Thesis: MULTI-INSECT VISUAL TRACKING AND SYSTEM IDENTIFICATION TECHNIQUES FOR INFLIGHT FEEDBACK INTERACTION ANALYSIS

Major Field: Mechanical and Aerospace Engineering

Biographical:

Education:

Completed the requirements for the Master of Science in Mechanical and Aerospace Engineering at Oklahoma State University, Stillwater, Oklahoma in July, 2021.

Completed the requirements for the Bachelor of Science in Mechanical Engineering at Bangladesh University of Engineering and Technology, Dhaka, Bangladesh in 2017.

Experience:

Graduate Research Assistant, Autonomous Physics Lab, Oklahoma State University.